Protein Folding

DOI: 10.1002/anie.200800298

Probing Protein–Chaperone Interactions with Single-Molecule Fluorescence Spectroscopy**

*Frank Hillger, Dominik Hänni, Daniel Nettels, Sonja Geister, Michelle Grandin, Marcus Textor, and Benjamin Schuler**

Molecular chaperones are an essential part of the cellular machinery that aids protein folding and assembly in vivo. Particularly remarkable are the members of the Hsp60 class, which encapsulate the folding protein in a central, closed cavity; the most well-studied example is the bacterial GroEL/ES system. Work of the past two decades has resolved many aspects of the processes involved.[1] However, remarkably little is known about the influence of the chaperone on the conformational distributions and folding mechanisms of its substrate proteins.[2] Because of the structural heterogeneity of the nonnative substrate bound to a molecular machine in the 10^6 Da range, its experimental investigation has been difficult with established ensemble methods.[2] Since single-molecule spectroscopy, in particular in combination with Förster resonance energy transfer (FRET), can provide distance and orientational information free of ensemble averaging[3] and allows intramolecular distance dynamics to be observed at equilibrium,[4,5] it is a promising approach to address such questions.[6] Herein, we show how single molecule FRET can be utilized to investigate the nonnative conformation and dynamics of bovine rhodanese, a classic chaperone substrate protein,[7,8] upon interaction with GroEL.

To obtain a transfer efficiency signature suitable for discriminating native and nonnative conformations, two rhodanese variants with complementary donor and acceptor positions (Figure 1) were investigated. Figure 1 c–j shows the transfer efficiency histograms determined from photon bursts originating from individual labeled rhodanese molecules freely diffusing through the observation volume of the confocal instrument. As expected, the rhodanese variant with the labels at the domain interface (Figure 1 a) shows a mean transfer efficiency $\langle E \rangle$ close to 1 in its native state (Figure 1 c); for the variant with labels at the ends of the interdomain linker (Figure 1 b), $\langle E \rangle = 0.69$ (Figure 1 d), which corresponds to a distance of 4.7 nm, in good agreement with the distance of 4.5 nm in the crystal structure.[9] In the unfolded state at 5 M guanidinium chloride (GdmCl), $\langle E \rangle$ scales with the sequence separation of the labeling sites (Figure 1 e,f), as expected.

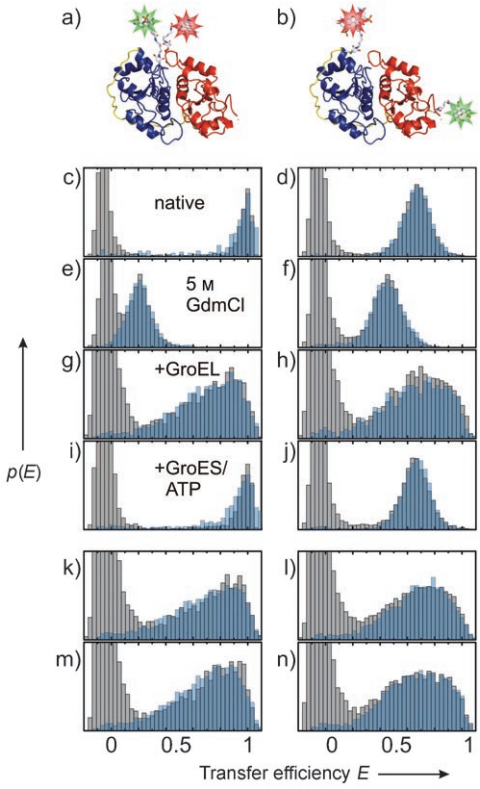

Figure 1. Native structures (based on PDB ID 1RHD) and transfer efficiency (E) histograms of rhodanese variants D102C–D219C (interface variant, panels on the left) and K135C–K174C (linker variant, panels on the right). a,b) Alexa Fluor 488 and Alexa Fluor 594 were coupled to the cysteine residues introduced by site-directed mutagenesis. c–j) E histograms of rhodanese variants under native (c,d) and denaturing conditions (5 M GdmCl, e,f), bound to GroEL upon dilution from GdmCl (g,h), and after refolding by addition of GroES/ATP (i,j), bound to GroEL after incubation with folded rhodanese at 30 °C for 16 h (k,l), and after dilution from 0.1 M phosphoric acid (m,n).The gray histograms were recorded with donor excitation only. For the blue histograms, pulsed interleaved excitation[14] was used. $p(E)$ = relative event frequency.

[*] Dr. F. Hillger, D. Hänni, Dr. D. Nettels, S. Geister, Prof. Dr. B. Schuler
Universität Zürich, Biochemisches Institut
8057 Zürich (Switzerland)
Fax: (+41) 44-635-5907
E-mail: schuler@bioc.uzh.ch
Homepage: http://www.bioc.uzh.ch/schuler
Dr. M. Grandin, Prof. Dr. M. Textor
ETH Zürich, Departement Materialwissenschaft
8093 Zürich (Switzerland)

[**] We thank A. Szabo for discussions and advice on anisotropy simulations, A. Plückthun and M. Kawe for discussions and samples of GroEL, H. Hofmann and D. Streich for discussions, the late P. Horowitz for a plasmid encoding rhodanese, and G. Lorimer for a plasmid encoding SR1. This work was supported by the VolkswagenStiftung, the Schweizerische Nationalfonds, the Swiss National Center of Competence in Research for Structural Biology, and the Human Frontier Science Program.

Supporting information for this article is available on the WWW under http://dx.doi.org/10.1002/anie.200800298.

Upon dilution of labeled rhodanese unfolded in GdmCl into buffer containing an excess of unlabeled GroEL, rhodanese becomes bound to the chaperone quantitatively, as evidenced by analytical size-exclusion chromatography (data not shown). We exclude the possibility of substrate protein binding to both chaperone rings by using the single-ring variant of GroEL, SR1,which binds to the substrate in a 1:1 complex.[10,11] Experiments with wild-type tetradecameric GroEL gave results essentially identical to the ones presented here. The transfer efficiency histograms of SR1-bound rhodanese (Figure 1 g,h) exhibit a pronounced broadening, indicating the presence of static heterogeneity on the observation time scale ($\approx$1 ms, duration of a fluorescence burst). For a random conformational distribution, we would expect a transfer efficiency that scales with the sequence separation of the dyes, as in the denaturant-unfolded state (Figure 1 e,f). In contrast, we observe maxima of the transfer efficiency histograms close to the values found in the native state (Figure 1 c,d), suggestive of a bias towards the native topology for rhodanese bound by the chaperone. The presence of very low intramolecular transfer efficiencies that could be hidden under the "donor only" peak[12] at $E \approx 0$ was excluded in experiments using alternating excitation of donor and acceptor[13,14] (Figure 1 c–n). The slight but reproducible difference in shape between the transfer efficiency histograms of the two chaperone-bound rhodanese variants (Figure 1 g,h) suggests that the E histograms provide a characteristic signature for the conformation of the substrate protein. Remarkably, the shapes of the transfer efficiency histograms are independent of how rhodanese is denatured (Figure 1 g,h,k–n), implying that the chaperone-bound conformation does not reflect the conformational distribution under unfolding conditions, but rather resembles a folding intermediate that is formed rapidly upon dilution into the SR1 solution (Figure 1 g,h,m,n), and that is also accessible from the native state under mildly destabilizing conditions (Figure 1 k,l).[15] After addition of ATP and the cochaperone GroES to the rhodanese–GroEL complex, the E distributions characteristic of the native structures are recovered[*] (Figure 1 c,d,i,j), demonstrating that labeled rhodanese is a fully functional chaperone substrate.

To probe the dynamics of the rhodanese–chaperone complex, we used correlation experiments employing a Hanbury Brown and Twiss setup.[4] Figure 2 a shows that rhodanese unfolded in 5 M GdmCl exhibits rapid intramolecular chain dynamics on a time scale of $\approx$70 ns. This time scale is very similar to that observed for the unfolded cold shock protein Csp*Tm*[4] and the Sup35 NM domain.[**][16] How do the dynamics of the denatured state change upon association with GroEL? The same measurement on rhodanese bound to GroEL yields a correlation with a decay of 0.2 μs (Figure 2 b), which at first sight could be misinterpreted as slowed distance dynamics. But the pronounced sensitivity of the correlation amplitude on the directions of polarization that are correlated (Figure S1 in the Supporting Information) indicates a strong contribution from rotational motion of the entire GroEL–rhodanese complex, which occurs exactly on this time scale.[*][18] To quantify the relative contributions of rotational and distance dynamics, we compare GroEL-bound rhodanese labeled with a FRET pair to GroEL-bound rhodanese labeled only with a donor chromophore. As shown in Figure 2 b, the two samples exhibit the same decay time of the correlation function. The ratio of the two correlations does not indicate the presence of an additional component (Figure 2 c), suggesting that the observed correlation is entirely due to rotation, and that distance dynamics are absent on this time scale. Additional evidence for the lack of distance dynamics comes from the pronounced intensity correlations of polarized acceptor emission upon donor excitation, which exhibit the same 0.2 μs decay (Figure S2 in the Supporting Information). This result shows that the relative orientation of donor and acceptor is rather invariant on this time scale, arguing that the same is true for their distance. The nanosecond chain

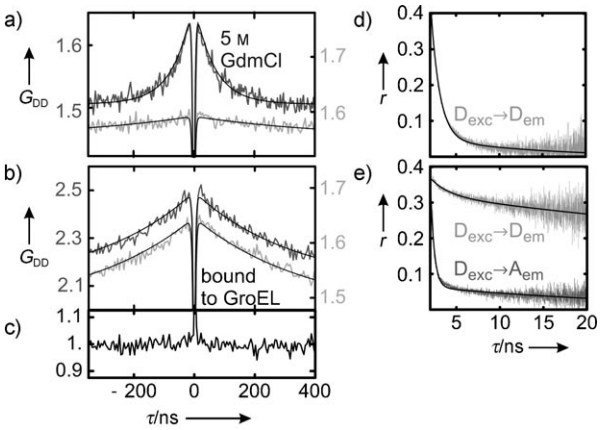

Figure 2. Dynamics of rhodanese. a–c) Donor–donor fluorescence intensity autocorrelation functions G_{DD} from Hanbury Brown and Twiss start–stop experiments.[4] Correlation functions are shown for the linker variant unfolded in 5 M GdmCl (a) and bound to GroEL (b). Dark gray lines show the correlation functions for the FRET-labeled, light gray lines for the donor-only-labeled rhodanese K174C. The black curves in (a) and (b) show fits to the correlation data including photon antibunching.[4] c) The normalized ratio of the two correlation functions from (b) indicates the absence of distance dynamics. d,e) Anisotropy decays for donor-only-labeled rhodanese K174C (light gray) under denaturing conditions (d) and bound to GroEL (e). The dark gray data in (e) show the fluorescence anisotropy decay of the acceptor upon excitation of the donor for the linker variant bound to GroEL. The black curves in (d) and (e) represent fits to Equation (1).

[*] Under our conditions, folded rhodanese is not confined within the cage.

[**] Note, however, that (in contrast to Csp*Tm*[4]), even singly labeled rhodanese exhibits some bunching on this time scale, albeit with lower amplitude (Figure 2 a), which complicates a quantitative analysis. This behavior is similar to recent observations for a Sup35 fragment, which were attributed to quenching of the fluorophores by aromatic residues in the chain.[16]

[*] In contrast to the magic angle configuration possible in conventional fluorimeters, the geometry of confocal epifluorescence instruments complicates the elimination of polarization effects on the correlation functions.[17]

dynamics observed in denaturant-unfolded rhodanese are thus suppressed when the protein is bound to the chaperone.

To investigate the presence of distance dynamics on longer time scales, we first employed subpopulation-specific fluorescence correlation spectroscopy on freely diffusing rhodanese–GroEL complexes (Figure 3). We correlated

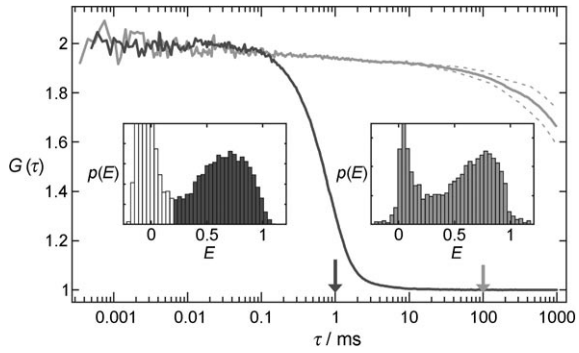

Figure 3. Normalized fluorescence intensity donor–acceptor cross-correlations and transfer efficiency histograms of the rhodanese-linker variant bound to GroEL (free diffusion: dark gray, surface-immobilized: light gray; corresponding binning times for *E* histograms indicated by arrows). Dashed lines indicate the individual cross-correlations (D→A and A→D, shown for $\tau > 0.5$ ms). For freely diffusing molecules, only events with $E > 0.2$ were used for the correlation (dark gray).

only signal from FRET-labeled molecules with $E > 0.2$ to minimize the contribution from donor-only labeled species, and we used donor–acceptor cross-correlation analysis to minimize the contribution of microsecond triplet dynamics.[19] Distance fluctuations would then result in an anticorrelated signal, that is, a rise in the correlation function. However, the correlation curves show no evidence for the presence of distance fluctuations up to ≈ 100 μs. To extend the accessible time scales beyond the diffusion time through the confocal volume, SR1–rhodanese complexes were immobilized on cover slides coated with biotinylated poly(L-lysine)-*graft*-poly(ethylene glycol) (PLL-*g*-PEG).[20] Individual complexes on the surface were identified by sample scanning and were observed individually for several seconds until the chromophores bleached. Surprisingly, donor–acceptor cross-correlation analysis of these data indicates the absence of long-range distance dynamics in chaperone-bound rhodanese even on long time scales. The decay of the correlation function setting in at times > 10 ms is caused by irreversible photobleaching, as indicated by the divergence of donor–acceptor and acceptor–donor cross-correlations (Figure 3).[21] The absence of large-amplitude distance fluctuations is also supported by the large width of transfer efficiency histograms from different observation or binning times (Figure 3, insets), indicating the presence of static heterogeneity on time scales up to at least 100 ms.

Finally, we need to establish the structural origin of the large width of the transfer efficiency distributions of chaperone-bound rhodanese (Figure 1). Static heterogeneity of the transfer rate can originate from either a distribution of intramolecular distances or a distribution of donor–acceptor orientations.[*] For rhodanese singly labeled with donor or acceptor and unfolded in 5 M GdmCl, the anisotropy decay $r(t)$ is dominated by a single component with a time constant of ≈ 1 ns (Figure 2d), indicating rapid and complete reorientation of the dyes, and thus justifying the common approximation of $\kappa^2 \approx 2/3$ for the orientational factor in Förster theory.[22] Upon binding to SR1, however, the anisotropy of all singly labeled variants (D102C, K135C, K174C, D219C) increases drastically, and the majority of the anisotropy decay occurs on the time scale of rotation of the entire rhodanese–SR1 complex (> 100 ns, Figure 2e). Consequently, the orientational restriction of the dyes must be taken into account to obtain distance information.

To this end, we analyze the fluorescence anisotropy decays of our singly labeled rhodanese variants with Equation (1), which describes the decay as the combined effect of restricted dye rotation (τ_{eff}) and the rotational motion of the entire protein–chaperone complex (τ_{M}).[23]

$$r(t) = \left((r_0 - r_\infty)e^{-t/\tau_{\text{eff}}} + r_\infty\right)e^{-t/\tau_{\text{eff}}} \quad (1)$$

Here, r_0 is the limiting anisotropy of the dyes,[**] and r_∞ is the residual anisotropy assuming no rotation of the macromolecule carrying the dye. Assuming restricted angular diffusion in a cone as the simplest plausible model for the motion of the chromophores[24] (Figure 4a), the semiangle $\Theta_{\max}$ of the cone can be calculated from Equation (2),[23,25] yielding for all our variants and dyes values between 17° and 19°.[***]

$$r_\infty = r_0\left(\frac{1}{2}\cos\Theta_{\max}(1+\cos\Theta_{\max})\right)^2 \quad (2)$$

Important additional information about the relative orientation of the dyes comes from the anisotropy decay of the acceptor upon donor excitation (Figure 2e): in this case, the residual anisotropy approaches zero for both chaperone-bound variants, indicating an angular distribution of the cone axes that is close to random. An alternative explanation, a narrow relative orientation close to the magic angle of 54.7°, can be excluded, because this would result in an apparent fundamental anisotropy of zero for the acceptor anisotropy decay upon donor excitation, which is incompatible with our obervations (Figure 2e). Additionally, a narrow distribution

[*] Heterogeneity in the quantum yields of the dyes originating, for example, from differences in the local environment can be excluded because of the agreement of fluorescence lifetimes (both in ensemble and single-molecule measurements) of the acceptor in FRET-labeled and the donor in singly labeled rhodanese on GroEL, respectively, with the lifetimes of the dyes on protein unfolded in 5 M GdmCl.

[**] $r_0 = 0.38$ was determined in a matrix of 99% glycerol at −10 °C.

[***] The lack of binding to GroEL of free dyes and several other small proteins and peptides labeled with the same dyes (size exclusion chromatography data not shown) indicates that the interaction of rhodanese with GroEL is dominated by the polypeptide and that the orientational restriction of the dyes results largely from steric constraints in the rhodanese–chaperone complex.

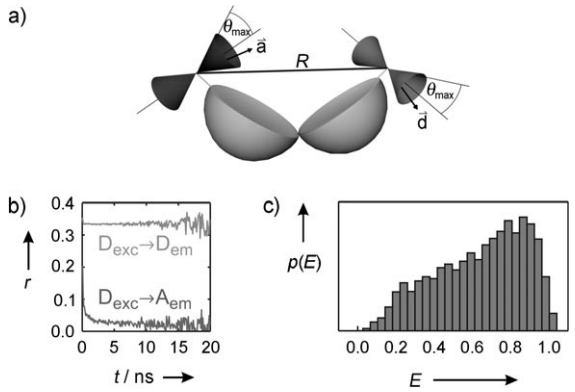

Figure 4. Simulations and structural interpretation. a) Assuming angular diffusion of the fluorophore dipoles $\vec{d}$ and $\vec{a}$ in cones of half angle Θ_{max} on the protein surface, and a narrow Gaussian distribution of distance *R*, we can account for both the characteristic anisotropy decays[34] (b) and the broad transfer efficiency histograms (c) observed experimentally (cf. Figures 1 and 2e). The two domains of rhodanese are indicated by the gray hemispheres in (a).

of relative orientations would at the same time require a broad distribution of distances to account for the broad transfer efficiency histograms we observe (Figure 1g,h,k–n), but this combination is physically implausible.

To interpret the experimental results quantitatively, we thus simulated the transfer process between orientationally restricted dipoles based on the simplest plausible model for our system (Figure 4): we assume that the relative orientation of the cones is fixed for every individual rhodanese–GroEL complex but randomly distributed from molecule to molecule. This assumption leads to anisotropy decays (Figure 4b) very similar to the experimental ones (Figure 2e), even for the characteristic decay of the acceptor anisotropy upon donor excitation. If we now assume a normal distribution of interdye distances *R* (Figure 4a) and adjust its mean and standard deviation to maximize the agreement between simulated and observed transfer efficiency histograms (Figure 4c and Figure S3 in the Supporting Information), we obtain distance distributions for GroEL-bound rhodanese with a mean distance of $\approx 4.5 \pm 0.5$ nm and a width of $\approx 0.5 \pm 0.2$ nm for both variants. For the linker variant, this is approximately the same value as in the native structure, but for the interface variant it is significantly larger, suggesting a large separation of the two rhodanese domains. If we used the mean distances for our two variants as constraints to adjust the relative orientation of the native domains, we would obtain a rhodanese conformation that is highly suggestive of binding to the rim of the GroEL ring, which is lined by hydrophobic residues that act as binding sites,[26] an arrangement that is in accord with a number of previous results.[27–29]

In summary, we have used a novel analysis combining time-resolved fluorescence anisotropy decays, single-molecule FRET experiments, and simulations to obtain quantitative information from a system with orientationally restricted chromophores, a situation that has been observed repeatedly in FRET experiments involving protein–chaperone interactions.[6,30] In our analyis, the donor and acceptor anisotropy decays define the opening angles of the cones constraining fluorophore rotation; the acceptor decay upon donor excitation constraines the relative orientational distribution of the cones; and the shape of the transfer efficiency histograms then define the mean and width of the distance distributions. What emerges from these measurements, together with the long-range dynamic information available from subpopulation-specific correlation functions, is the picture of a rather well-defined ensemble of rhodanese conformations that resembles a partially structured folding intermediate when bound to the chaperone GroEL. Interestingly, the lack of long-range distance dynamics does not seem to preclude local structural fluctuations evident from protease susceptibility,[27,28] or NMR[18,31] or fluorescence spectroscopy.[8,27] Our results illustrate the potential for extracting quantitative structural information from FRET experiments even in cases where large anisotropies demand that orientational effects be taken into account, and provide an important step towards investigating the role of cellular factors in protein folding.

Experimental Section

Proteins were prepared as described previously.[10,32] Binding of rhodanese to SR1 was achieved as follows: A) Rhodanese unfolded in 5 M GdmCl was rapidly diluted tenfold into folding buffer (0.1 M potassium phosphate, 5 mM magnesium chloride, 200 mM 2-mercaptoethanol, 0.001 % Tween 20, 1 mM EDTA, pH 7.0) containing at least a tenfold molar excess of SR1 heptamers. B) Same as (A), but unfolding was carried out in 0.1 M phosphoric acid. C) Rhodanese was incubated at 30 °C for 16 h in folding buffer with a tenfold molar excess of SR1 heptamers. Complete binding was assessed on a TSK 5000 PWXL column (TOSOH Bioscience) with fluorescence detection.

For surface immobilization, SR1 was biotinylated using (+)-biotin *N*-hydroxysuccinimide ester in a molar ratio of 1:7. A solution of 0.1 mg mL^{-1} PLL(20)-g[3.5]-PEG(2)/PEG(3.4)-biotin (50 %)[20] in 10 mM potassium phosphate, pH 7.0, was applied to a custom-made quartz flow cell. After 15 min of incubation, the flow cell was washed with 0.1 M potassium phosphate, 5 mM magnesium chloride, 1 mM EDTA, pH 7.0; then 1 mg mL^{-1} avidin was applied in the same buffer. After 15 min of incubation, the flow cell was washed thoroughly, and 250–500 nM GroEL–rhodanese preparation was applied. The cell was incubated for 5 min and then washed with buffer.

Anisotropy decay data were recorded with a custom-built fluorescence lifetime spectrometer using 1 μM samples of labeled protein. Single-molecule FRET measurements were performed as previously described[4,32,33] using an adapted MicroTime 200 confocal microscope (PicoQuant, Berlin). For additional details, see the Supporting Information.

Received: January 21, 2008
Revised: April 29, 2008
Published online: July 10, 2008

Keywords: chaperones · correlation spectroscopy · FRET · protein folding · single-molecule studies

[1] D. Thirumalai, G. H. Lorimer, *Annu. Rev. Biophys. Biomol. Struct.* **2001**, *30*, 245–269; H. Grallert, J. Buchner, *J. Struct. Biol.* **2001**, *135*, 95–103; J. C. Young, V. R. Agashe, K. Siegers, F. U. Hartl, *Nat. Rev. Mol. Cell Biol.* **2004**, *5*, 781–791; A. L. Horwich, G. W. Farr, W. A. Fenton, *Chem. Rev.* **2006**, *106*, 1917–1930.

[2] W. A. Fenton, A. L. Horwich, *Q. Rev. Biophys.* **2003**, *36*, 229–256.
[3] G. Haran, *J. Phys. Condens. Matter* **2003**, *15*, R1291–R1317; B. Schuler, *ChemPhysChem* **2005**, *6*, 1206–1220; X. Michalet, S. Weiss, M. Jäger, *Chem. Rev.* **2006**, *106*, 1785–1813; B. Schuler, W. A. Eaton, *Curr. Opin. Struct. Biol.* **2008**, *18*, 16–26.
[4] D. Nettels, I. V. Gopich, A. Hoffmann, B. Schuler, *Proc. Natl. Acad. Sci. USA* **2007**, *104*, 2655–2660.
[5] E. V. Kuzmenkina, C. D. Heyes, G. U. Nienhaus, *Proc. Natl. Acad. Sci. USA* **2005**, *102*, 15471–15476.
[6] S. Sharma, K. Chakraborty, B. K. Müller, N. Astola, Y. C. Tang, D. C. Lamb, M. Hayer-Hartl, F. U. Hartl, *Cell* **2008**, *133*, 142–153.
[7] J. A. Mendoza, E. Rogers, G. H. Lorimer, P. M. Horowitz, *J. Biol. Chem.* **1991**, *266*, 13044–13049.
[8] J. Martin, T. Langer, R. Boteva, A. Schramel, A. L. Horwich, F. U. Hartl, *Nature* **1991**, *352*, 36–42.
[9] J. H. Ploegman, G. Drent, K. H. Kalk, W. G. J. Hol, *J. Mol. Biol.* **1978**, *123*, 557–594.
[10] A. L. Horwich, S. G. Burston, H. S. Rye, J. S. Weissman, W. A. Fenton, *Methods Enzymol.* **1998**, *290*, 141–146.
[11] J. S. Weissman, H. S. Rye, W. A. Fenton, J. M. Beechem, A. L. Horwich, *Cell* **1996**, *84*, 481–490.
[12] B. Schuler, E. A. Lipman, P. J. Steinbach, M. Kumke, W. A. Eaton, *Proc. Natl. Acad. Sci. USA* **2005**, *102*, 2754–2759.
[13] A. N. Kapanidis, N. K. Lee, T. A. Laurence, S. Doose, E. Margeat, S. Weiss, *Proc. Natl. Acad. Sci. USA* **2004**, *101*, 8936–8941.
[14] B. K. Müller, E. Zaychikov, C. Bräuchle, D. C. Lamb, *Biophys. J.* **2005**, *89*, 3508–3522.
[15] T. Shibatani, G. Kramer, B. Hardesty, P. M. Horowitz, *J. Biol. Chem.* **1999**, *274*, 33795–33799; K. E. Smith, P. A. Voziyan, M. T. Fisher, *J. Biol. Chem.* **1998**, *273*, 28677–28681.
[16] S. Mukhopadhyay, R. Krishnan, E. A. Lemke, S. Lindquist, A. A. Deniz, *Proc. Natl. Acad. Sci. USA* **2007**, *104*, 2649–2654.
[17] Ü. Mets in *Fluorescence Correlation Spectroscopy* (Eds.: E. S. Elson, R. Rigler), Springer, Berlin, **2001**.
[18] R. Horst, E. B. Bertelsen, J. Fiaux, G. Wider, A. L. Horwich, K. Wüthrich, *Proc. Natl. Acad. Sci. USA* **2005**, *102*, 12748–12753.
[19] P. Schwille in *Fluorescence Correlation Spectroscopy* (Eds.: E. S. Elson, R. Rigler), Springer, Berlin, **2001**; C. Eggeling, P. Kask, D. Winkler, S. Jäger, *Biophys. J.* **2005**, *89*, 605–618.
[20] N. P. Huang, J. Vörös, S. M. De Paul, M. Textor, N. D. Spencer, *Langmuir* **2002**, *18*, 220–230.
[21] C. Eggeling, J. Widengren, L. Brand, J. Schaffer, S. Felekyan, C. A. M. Seidel, *J. Phys. Chem. A* **2006**, *110*, 2979–2995.
[22] B. W. Van Der Meer, G. Coker III, S. Y. S. Chen, *Resonance Energy Transfer: Theory and Data*, VCH, New York, **1994**.
[23] G. Lipari, A. Szabo, *Biophys. J.* **1980**, *30*, 489–506.
[24] G. F. Schröder, U. Alexiev, H. Grubmüller, *Biophys. J.* **2005**, *89*, 3757–3770.
[25] K. Kinosita, S. Kawato, A. Ikegami, *Biophys. J.* **1977**, *20*, 289–305.
[26] K. Braig, Z. Otwinowski, R. Hegde, D. C. Boisvert, A. Joachimiak, A. L. Horwich, P. B. Sigler, *Nature* **1994**, *371*, 578–586.
[27] J. A. Mendoza, M. C. Butler, P. M. Horowitz, *J. Biol. Chem.* **1992**, *267*, 24648–24654.
[28] R. Hlodan, P. Tempst, F. U. Hartl, *Nat. Struct. Biol.* **1995**, *2*, 587–595.
[29] P. Thiyagarajan, S. J. Henderson, A. Joachimiak, *Structure* **1996**, *4*, 79–88; A. van der Vaart, J. P. Ma, M. Karplus, *Biophys. J.* **2004**, *87*, 562–573; G. W. Farr, K. Furtak, M. B. Rowland, N. A. Ranson, H. R. Saibil, T. Kirchhausen, A. L. Horwich, *Cell* **2000**, *100*, 561–573.
[30] Z. Lin, H. S. Rye, *Mol. Cell* **2004**, *16*, 23–34.
[31] R. Zahn, S. Perrett, G. Stenberg, A. R. Fersht, *Science* **1996**, *271*, 642–645; R. Zahn, C. Spitzfaden, M. Ottiger, K. Wüthrich, A. Plückthun, *Nature* **1994**, *368*, 261–265.
[32] F. Hillger, D. Nettels, S. Dorsch, B. Schuler, *J. Fluoresc.* **2007**, *17*, 759–765.
[33] A. Hoffmann, A. Kane, D. Nettels, D. E. Hertzog, P. Baumgärtel, J. Lengefeld, G. Reichardt, D. A. Horsley, R. Seckler, O. Bakajin, B. Schuler, *Proc. Natl. Acad. Sci. USA* **2007**, *104*, 105–110.
[34] Rotation of the rhodanese-GroEL complex was not included in the simulations, which therefore lack the slow relaxation component ($\tau_M = \infty$ in Eq. 1).

Angewandte Chemie
Eine Zeitschrift der Gesellschaft Deutscher Chemiker

Supporting Information

69451 Weinheim, Germany

Supporting information

Probing protein-chaperone interactions with single molecule fluorescence spectroscopy

Frank Hillger, Dominik Hänni, Daniel Nettels, Sonja Geister, Michelle Grandin, Marcus Textor, and Benjamin Schuler

Materials and Methods

Protein Preparation and Labeling. Cysteine variants of rhodanese were prepared and labeled with Alexa 488 and Alexa 594 (R_0 = 5.4 nm) as described previously[1]. Cysteine residues were introduced by site-directed mutagenesis at positions 135 and 174 ("linker variant") and 102 and 219 ("interface variant"), respectively. After labeling, thiosulfate was removed from the active site of rhodanese by reaction with potassium cyanide and subsequent size exclusion chromatography. GroEL-SR1 was expressed and purified essentially as described by Horwich *et al.*[2] and stored at -80 °C as a suspension of precipitate in 2.7 M ammonium sulfate.

Preparation of Rhodanese-Chaperone Complexes. SR1 ammonium sulfate precipitate was resolubilized at 10 to 20 μM SR1 (heptamer) in folding buffer (0.1 M potassium phosphate (Fluka Ultra), 5 mM magnesium chloride (Roth), 200 mM 2-mercaptoethanol (Fluka Ultra), 0.001 % Tween 20 (Pierce), 1 mM EDTA (Biosolve), pH 7.0). Binding of rhodanese to SR1 was achieved as follows: **A**) Rhodanese unfolded in 5 M GdmCl (Pierce), 0.1 M potassium phosphate, 200 mM 2-mercaptoethanol, 0.001 % Tween 20, 1 mM EDTA, pH 7.0 was rapidly diluted tenfold into folding buffer containing at least a tenfold molar excess of SR1 heptamers. **B**) As **A,** but unfolding was carried out by tenfold dilution of native rhodanese into 0.1 M phosphoric acid. **C**) Rhodanese was incubated at 30 °C over night in folding buffer containing a 10-fold molar excess of SR1 heptamers. Complete binding was assessed by analytical size exclusion chromatography on a TSK 5000 PWXL (TOSOH Bioscience) and fluorescence detection. In all cases, rhodanese was bound completely to SR1. Single-molecule experiments and size exclusion chromatography indicated the absence of unbound rhodanese molecules or aggregates[1].

Note that rhodanese shows a pronounced collapse upon dilution from denaturant within the dead time of ensemble stopped-flow mixing experiments, indicating the formation of a compact structural ensemble before the slower phases of folding ensue. The dominant phase of refolding for our labeled rhodanese variants occurs with half times of ~15 min, within the range of reactivation times of unlabeled rhodanese reported in the literature[3], suggesting that labeling does not strongly interfere with the folding mechanism. The widths of the transfer efficiency histograms (Fig. 1 main text) for native, unfolded, and refolded rhodanese interface variant were 0.08±0.01, 0.08±0.01, and 0.10±0.01, respectively, and for the linker variant 0.11±0.01, 0.10±0.01, and 0.10±0.01, respectively. At the exceedingly low protein concentrations used in our experiments, aggregation rates become negligible and the native state is reached reversibly upon refolding also in the absence of GroEL/ES.

Biotinylation and Surface Immobilization of GroEL/SR1. Ammonium sulfate-precipitated SR1 was transferred to 100 mM $NaHCO_3$ (Roth) using a 5 ml HiTrap desalting column (GE Amersham), followed by concentration to 30-40 mg/ml in Centricon YM-3 filter devices (Amicon). (+)-Biotin N-hydroxy-succinimide ester (Sigma) was dissolved in dry DMSO (Pierce) and added to concentrated SR1 in a molar ratio of 1 to 7. After incubation for 4 hours, the reaction mixture was purified and transferred to 0.1 M potassium phosphate (Fluka Ultra), 5 mM magnesium chloride (Roth), 1 mM EDTA (Biosolve), pH 7.0, using a Superdex 200 10/300 GL (Amersham) gel filtration column. Biotinylation was analyzed using ESI TOF mass spectroscopy and samples were stored at 5 mg/ml at -80 °C. 0.1 mg/ml PLL(20)-g[3.5]-PEG(2)/PEG(3.4)-Biotin (50%)[4] was dissolved in 10 mM potassium phosphate (Fluka Ultra), pH 7.0, and applied to a custom-made quartz flow cell. After 15 min of incubation, the flow cell was washed with 0.1 M potassium phosphate (Fluka Ultra), 5 mM magnesium chloride (Roth), 1 mM EDTA (Biosolve), pH 7.0, then 1 mg/ml Avidin D (Vector) were applied in the same buffer. After 15 min of incubation, the flow cell was washed vigorously. The GroEL/rhodanese complex was prepared as described above and separated from monomeric rhodanese and rhodanese aggregates by size exclusion chromatography. 250-500 nM of GroEL/rhodanese preparation were applied to the flow cell and incubated for 5 min before the cell was washed with buffer.

Single Molecule Fluorescence Spectroscopy. Observations of single-molecule fluorescence were made using a MicroTime 200 confocal single molecule instrument (PicoQuant, Berlin, Germany) equipped with a Olympus UplanApo 60x/1.20W objective and four detection channels. Donor excitation pulses of 470 nm wavelength are generated by a diode laser (LDH 470, PicoQuant). Except for PIE measurements (see below) the pulse repetition rate was 40 MHz, resulting in an average power of 100 µW entering the completely illuminated back aperture of the objective. Laser light and fluorescence emission are separated using a dual band beam splitter (z488/568, Chroma), followed by a 100 µm pinhole. Sample fluorescence was further separated by a polarizing beam splitter cube into components parallel and perpendicular polarized with respect to the excitation light. Subsequently, both components were further divided into donor and acceptor photons by means of dichroic mirrors (585DCXR, Chroma), filtered (donor emission filters: Chroma HQ525/50, Omega 525AF45, acceptor emission filters: Chroma HQ650/100 and HQ600LP), and focused on avalanche photodiodes (PerkinElmer Optoelectronics SPCM-AQR-15). A TimeHarp 200 counting card (PicoQuant) records the arrival time of every detected photon with a time resolution of 100 ns. In addition, the time separation between excitation pulse and photon detection is stored with 38 ps resolution. For pulsed interleaved excitation[5] PIE, the wavelength range used for acceptor excitation was selected with a z582/15 band pass filter (Chroma) from the emission of an SC-450-4 supercontinuum fiber laser (Fianium, UK) driven at 15 MHz. The emission is monitored by a fast photodiode (DET10A/M, Thorlabs), which triggers the LDH 470 driver to deliver single laser pulses. The time separation between the acceptor and donor excitation pulses of 33 ns was adjusted with a delay line. FCS data down to 0.1 µs lag time (Fig. 3) were recorded and calculated using the software SymphoTime (PicoQuant). Fluorescence correlation data in the sub-microsecond range (down to 256 ps lag time, Fig. 2) were recorded and analyzed as described previously using a Hanbury Brown and Twiss detection scheme[6],

a continuous wave solid-state diode-pumped laser (Coherent Sapphire 488-200) operating at 488 nm (average radiant power at the sample: 100μW) and a PicoHarp 300 or a HydraHarp 400 photon counting module (PicoQuant). Subpopulation-specific donor-acceptor cross-correlations were obtained by correlating only photons from bursts assigned to the unfolded subpopulation.

For experiments on surface-immobilized molecules, the MicroTime 200 (PicoQuant) was used in combination with a 488 nm cw laser. Sample scanning with an x/y-piezo-stage (P-733 and E-710, Physik Instrumente) in combination with custom-developed software allowed the automated identification and data acquisition of immobilized molecules. In area scans over regions of $80\times80\,\mu\text{m}^2$ (0.156 nm point resolution, 5 μW average radiant power at the sample), the locations of the individual molecules were identified and measured for five seconds each. For the data shown in Fig. 2 of the main text, 1297 trajectories were analyzed. To quantify the background intensity, 30 trajectories were measured at positions lacking labeled protein.

Single Molecule Data Reduction and Analysis. Successive photons detected in any channel and separated by less than 100 μs were combined into one burst. A burst was retained as a significant event if the total number of counts exceeded 50 (after correction for background, differences in quantum yields, the different collection efficiencies of the detection channels, cross-talk, and direct excitation of the acceptor)[7]. In addition, bursts with a significant likelihood for acceptor photobleaching during the burst were discarded (see below). Transfer efficiencies were calculated as $E = n_A/(n_D + n_A)$, where n_D and n_A are the corrected donor and acceptor counts of each burst.

For calculating correlation functions from measurements on immobilized molecules, the trajectories were merged and donor and acceptor intensities cross-correlated. For normalization, each correlation was divided by the mean fluorescence calculated from the first 10 data points of each correlation. For transfer efficiency histograms, the trajectory data were binned in 100 ms intervals and corrected for background. For each trajectory the maximum change in the sum of donor and acceptor fluorescence signal was calculated and only trajectories were selected were this difference was >200 counts and did not exceed 1200 counts. The trajectories were truncated at 1 s to minimize the contribution of background. Transfer efficiency histograms were calculated for each bin of the trajectories using $E = n_A/(n_A + \gamma\, n_D)$, where $\gamma = 1.2$ corrects for the difference in quantum yield of donor and acceptor dyes as well as the detection efficiencies of the channels.

Identification of Fluorescence Bursts Affected by Photobleaching. Assume that during a burst of duration T, n_D donor photons and n_A acceptor photons were detected at times $t_{D,1}\ldots t_{D,n_D}$ and $t_{A,1}\ldots t_{A,n_A}$, respectively. With the average values $\overline{t}_D = 1/n_D\sum_i t_{D,i}$ and $\overline{t}_A = 1/n_A\sum_i t_{A,i}$, we define the burst asymmetry as $\alpha_{DA} = \overline{t}_D - \overline{t}_A$. In the limit of $n_D, n_A \to \infty$, the asymmetry is zero if donor and acceptor dyes emit photons continuously with rates, $\tau_{D,A}^{-1} = n_{D,A}/T$, during the complete burst duration T. However, if the acceptor dye bleaches at a certain time during the photon burst, the acceptor photon rate will drop to the background level, and the donor rate will increase due to the interrupted energy transfer, resulting in a

burst asymmetry $\alpha_{DA} > 0$. For finite photon numbers n_D and n_A, shot noise of the calculated α_{DA} has to be taken into account. Here we calculate the standard deviation of α_{DA} for the ideal case that no photobleaching occurs during the burst. For a randomly chosen burst photon i, the detection time t_i is then uniformly distributed, with a constant probability density function $p(t_i) = 1/T$, such that $\int_0^T p(t_i)dt_i = 1$. The expectation value for t_i is then $\overline{t_i} = \int_0^T t_i\, p(t_i)dt_i = T/2$ and the variance is $\sigma_i^2 = \int_0^T (t_i - \overline{t_i})^2\, p(t_i)dt_i = T^2/12$. With these relations, the variance of $\overline{t_D}$ and $\overline{t_A}$ defined above result as $\Delta\overline{t}_{D,A}{}^2 = \sum_i \sigma_i^2 / n_{D,A}^2 = T^2/12n_{D,A}$. Finally, we obtain for the standard deviation of α_{DA}:

$$\sigma_{DA} = \frac{T}{2\sqrt{3}}\left(\frac{1}{n_D} + \frac{1}{n_A}\right)^{1/2}. \qquad (1)$$

This approximation is valid if the dead time of the detectors (≈ 100 ns) is short compared to the inter-photon times $\tau_{D,A}$ during the bursts (on average ~10 μs). To exclude bursts with a significant deviation of α_{DA} from zero, indicating that a bleaching process is likely to have occurred, bursts with $|\alpha_{DA}| > \sigma_{DA}$ were not included in the analysis. An example of the analysis is shown in Fig. S4.

Time-Resolved Anisotropy. Anisotropy decay data were recorded with a custom-built fluorescence lifetime spectrometer using samples of 1 μM labeled protein. The fluorophores were excited at 470 nm by vertically polarized laser pulses with 20 MHz repetition rate. Collimated fluorescence light, emitted in perpendicular direction with respect to the laser beam, passed an analyzing Glan-Thompson polarizer and a band pass filter (525AF45, Omega Filters, or HQ640/100, Chroma) before it was focused onto a microchannel plate photomultiplier tube (PMT R3809U-50, Hamamatsu). The output pulses of the PMT were pre-amplified (PAM 102-M, PicoQuant), and times between laser pulses and fluorescence photon arrival times were recorded by a photon counting module (PicoHarp 300, PicoQuant). Fluorescence decay histograms with 8 ps bin width were formed. The overall instrument response function (IRF) of the system was measured to have a FWHM of $\Delta_{IRF} = 80$ ps. Two fluorescence decays $I_V(t)$ and $I_H(t)$ were measured for each sample with the analyzing polarizer in vertical and in horizontal orientation, respectively. From these decays the anisotropy as a function of time was determined as

$$r(t) = \frac{I_V(t) - GI_H(t)}{I_V(t) + 2GI_H(t)},$$

where G is a correction factor compensating for the slightly different instrumental detection sensitivity for vertically and horizontally polarized photons.

Simulations. Resonance energy transfer in the presence of orientational constraints of donor and acceptor dyes was simulated using Mathematica (Wolfram Research) as follows. The orientational dynamics of the fluorophores were modeled as angular diffusion of the dye dipole in a cone[8], approximated by a random walk on the corresponding segment of a unit sphere[9]. For every simulated fluorescence burst, corresponding to an individual rhodanese-GroEL complex, we assumed a random, isotropic, but fixed, relative orientation of the cone

axes for donor and acceptor, separated by a distance selected randomly from a normal distribution of given mean and standard deviation. The Brownian dynamics for the diffusive motion of the dye dipoles were combined with a Monte Carlo simulation of the photon emission process of the coupled dye pair[10]. After each time step of 10 ps, the transfer efficiency was calculated from the distance and the relative orientation of donor and acceptor dipoles[11]. For each emitted photon, the orientation of the donor dye at the time of absorption, the orientation of the emitting dye at the time of emission, and the time interval between donor excitation and photon emission were stored for the calculation of anisotropy decays. Each calculation consisted of 5000 simulated bursts of 50 photons each (corresponding to 5000 rhodanese-GroEL complexes with different relative cone orientations) to achieve similar statistics as in the experiment. From the complete data set, transfer efficiency histograms and anisotropy decays were calculated as shown in Figs. 4 and S3.

Supporting Figures

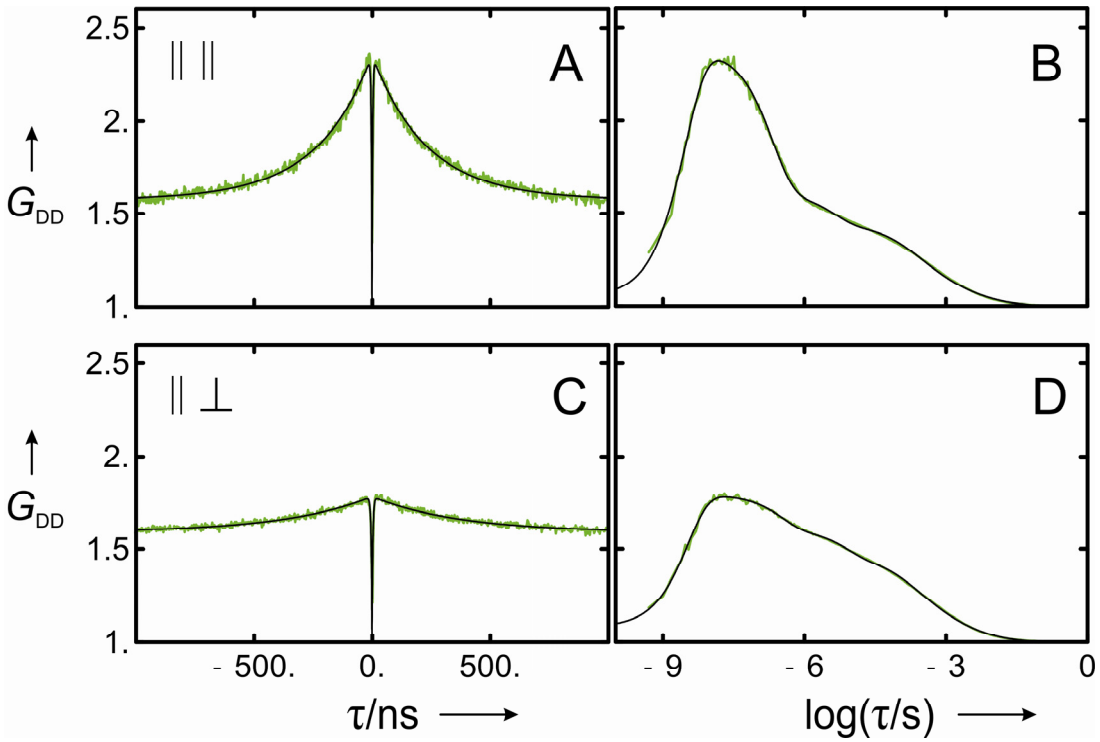

Fig. S1. *Dependence of the donor intensity autocorrelation function of GroEL-bound rhodanese on the polarizations used for signal correlation*. (A,B) Donor (horizontal polarization) – donor (horizontal polarization) intensity correlation of donor-only-labeled rhodanese bound to GroEL. (C,D) Donor (horizontal polarization) – donor (vertical polarization) intensity correlation. The pronounced difference in amplitude indicates that the correlation is caused by rotational motion of the entire rhodanese-chaperone complex[12]. The relative amplitudes are in good agreement with theoretical calculations of the polarization dependence[13] (not shown).

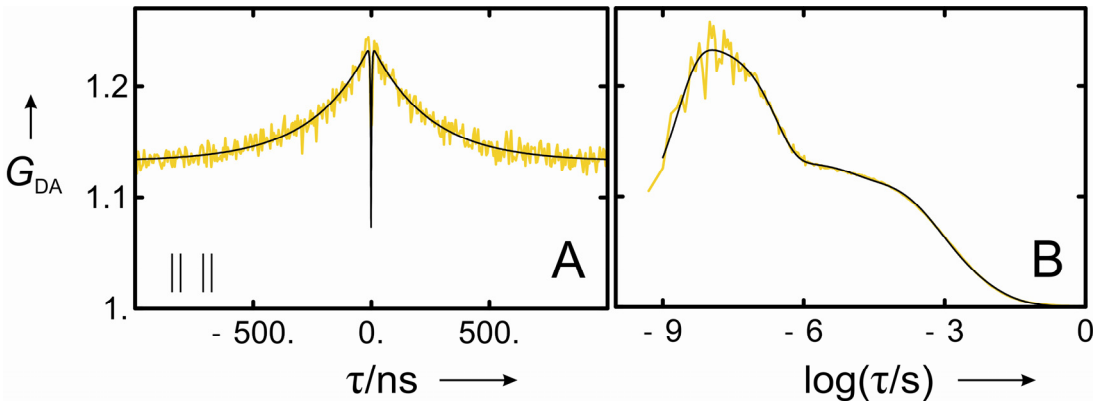

Fig. S2. *Donor (horizontal polarization)-acceptor (horizontal polarization) crosscorrelation of FRET-labeled chaperone-bound rhodanese.* The pronounced correlation on the timescale of rotational diffusion of the entire rhodanese-chaperone complex (A: linear, B: logarithmic scale) shows that the relative orientation of donor and acceptor chromophores in the chaperone-bound protein is rather fixed on the time scale of ~0.2 μs, such that a marked polarization component is retained in spite of energy transfer, implying that the intramolecular distance between the dyes also does not change on this time scale.

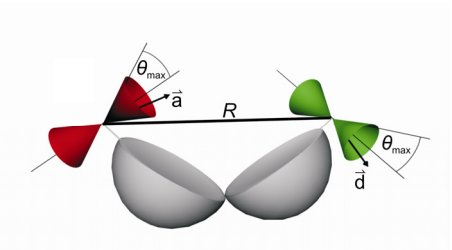

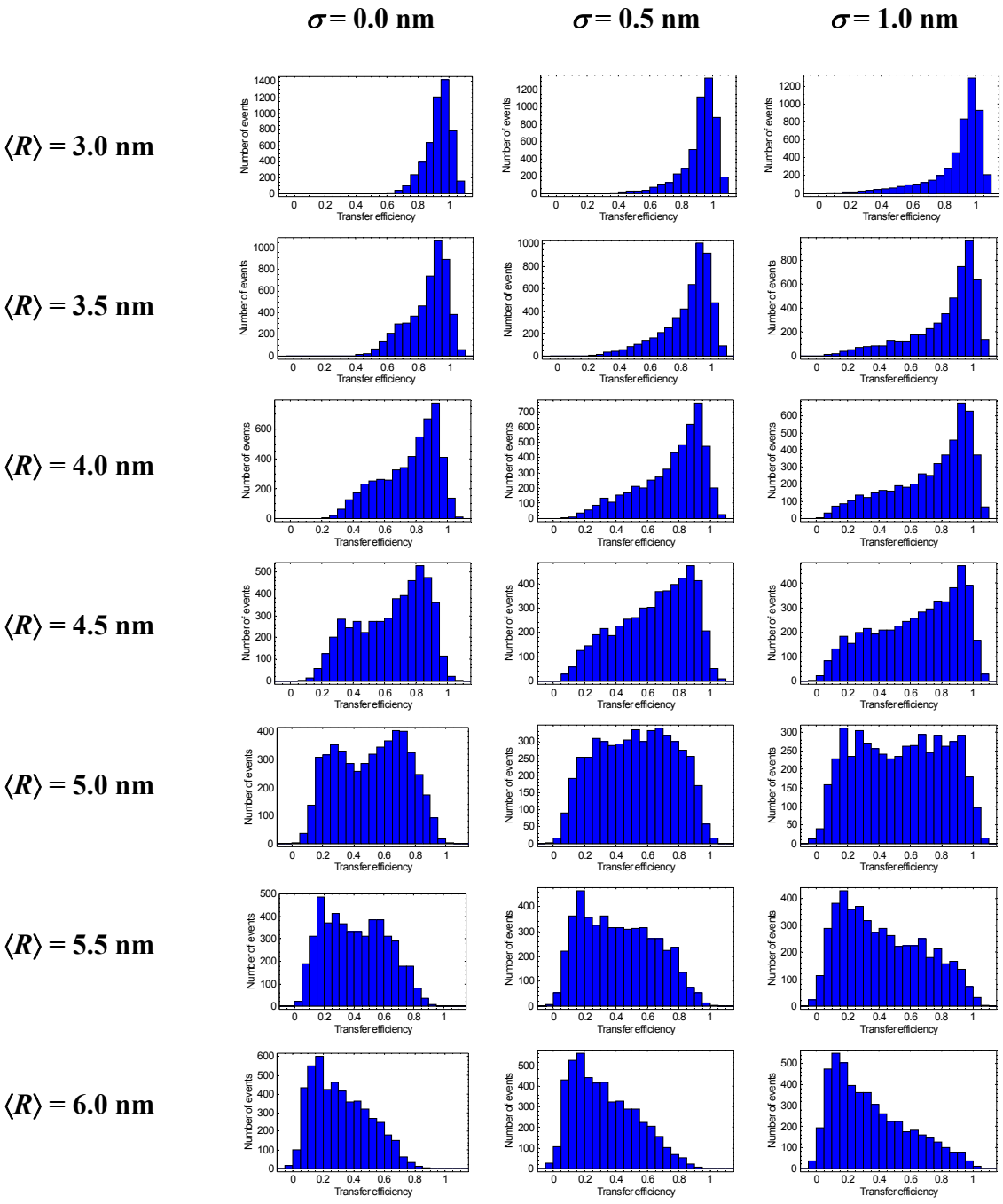

Fig. S3. *Simulated transfer efficiency histograms* with systematic variation of the distance distribution between donor and acceptor, assuming orientational restriction of the dyes as described in the main text and *Experimental Section*. Realistic background values were included for the calculation of the histograms. The shape of the histograms is very sensitive to the mean distance $\langle R \rangle$ and the width (standard deviation σ) of the distance distribution (here assumed to be Gaussian). Note in particular that for very short distances the transfer efficiency distribution is very narrow and close to $E = 1$. The Förster radius R_0 is 5.4 nm.

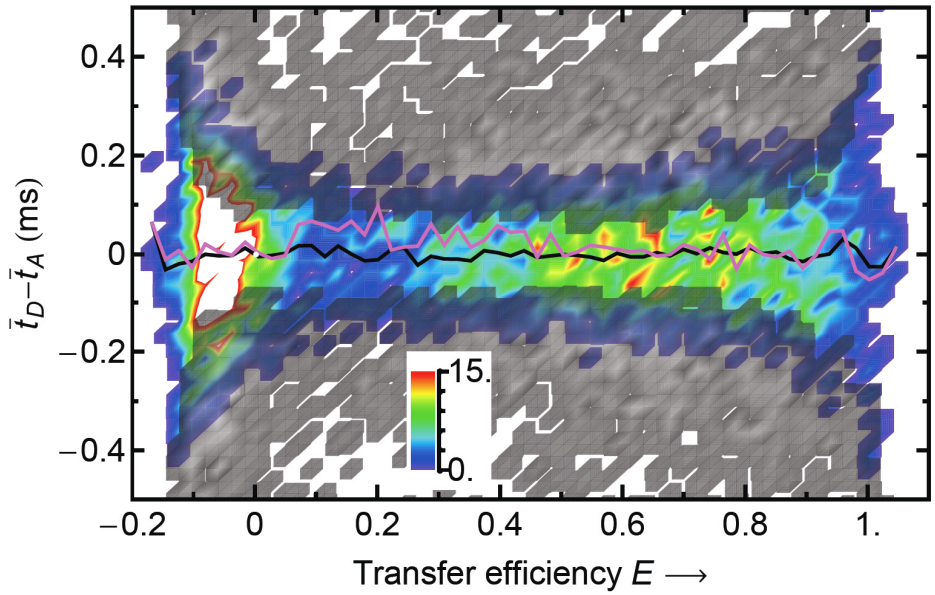

Fig. S4. *Identification of Fluorescence Bursts Affected by Photobleaching.* The burst asymmetry α is shown as a function of the FRET efficiency. The events with $|\alpha_{DA}| > \sigma_{DA}$ are shown in grey, the intensity scale for the remaining events is shown in color. The mean burst asymmetries before and after eliminating the asymmetric events are shown in purple and black, respectively, indicating exclusion of bursts where the acceptor was photobleached during the transit through the confocal volume.

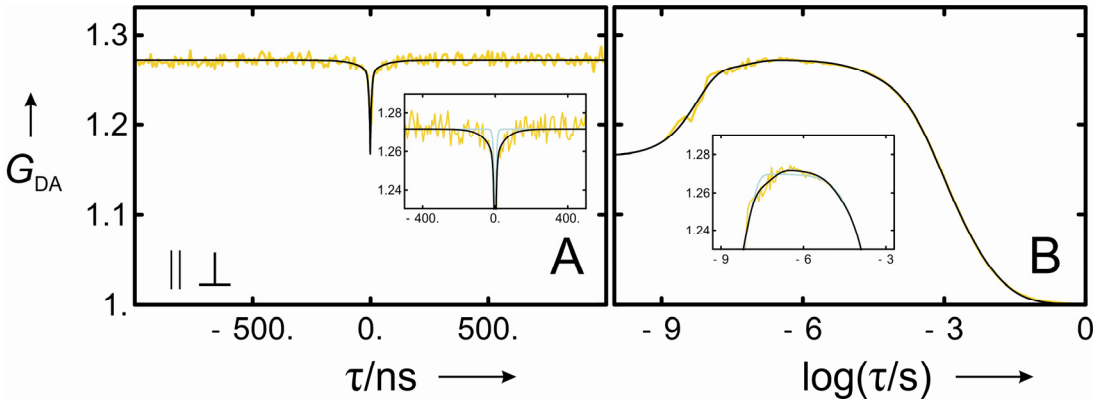

Fig. S5. *Anticorrelation of the Donor (horizontal polarization) - acceptor (vertical polarization) crosscorrelation caused by intramolecular dynamics of rhodanese in 5 M GdmCl.* (A) Short time correlation with linear time base including a fit to the data resulting in a time constant of 80 ns for intramolecular dynamics, in good agreement with the autocorrelation data (Fig. 2 main text). (Inset) Comparison of fits including (black) and excluding (green) distance dynamics. (B) Complete correlation function with logarithmic time base. Fits and inset analogous to (A).

References

[1] F. Hillger, D. Nettels, S. Dorsch, B. Schuler, *J. Fluoresc.* **2007**, *17*, 759-765.

[2] A. L. Horwich, S. G. Burston, H. S. Rye, J. S. Weissman, W. A. Fenton, *Methods Enzymol.* **1998**, *290*, 141-6.

[3] A. M. Bhattacharyya, P. M. Horowitz, *J. Biol. Chem.* **2001**, *276*, 28739-43; J. A. Mendoza, E. Rogers, G. H. Lorimer, P. M. Horowitz, *J. Biol. Chem.* **1991**, *266*, 13044-13049; B. M. Gorovits, P. M. Horowitz, *Biochemistry* **1998**, *37*, 6132-5; G. Zardeneta, P. M. Horowitz, *J Biol Chem* **1992**, *267*, 5811-6.

[4] N. P. Huang, J. Vörös, S. M. De Paul, M. Textor, N. D. Spencer, *Langmuir* **2002**, *18*, 220-230.

[5] B. K. Müller, E. Zaychikov, C. Bräuchle, D. C. Lamb, *Biophys. J.* **2005**, *89*, 3508-3522.

[6] D. Nettels, I. V. Gopich, A. Hoffmann, B. Schuler, *Proc. Natl. Acad. Sci. USA* **2007**, *104*, 2655-2660.

[7] B. Schuler, *Methods. Mol. Biol.* **2007**, *350*, 115-38.

[8] G. Lipari, A. Szabo, *Biophys. J.* **1980**, *30*, 489-506; K. Kinosita, S. Kawato, A. Ikegami, *Biophys. J.* **1977**, *20*, 289-305; G. F. Schröder, U. Alexiev, H. Grubmüller, *Biophys J* **2005**, *89*, 3757-3770.

[9] J. B. Pedersen, *J. Chem. Phys.* **1972**, *57*, 2680-&.

[10] Z. S. Wang, D. E. Makarov, *J. Phys. Chem. B* **2003**, *107*, 5617-5622.

[11] B. W. Van Der Meer, Coker, G. III, Chen, S. Y. S., *Resonance energy transfer: theory and data*, VCH Publishers, Inc., New York, **1994**.

[12] Ü. Mets, in *Fluorescence Correlation Spectroscopy* (Eds.: E. S. Elson, R. Rigler), Springer-Verlag, Berlin, **2001**.

[13] P. Kask, P. Piksarv, M. Pooga, Ü. Mets, E. Lippmaa, *Biophys. J.* **1989**, *55*, 213-220.